Polymer Chemistry

ROYAL SOCIETY OF CHEMISTRY

PAPER

View Article Online
View Journal

Cite this: DOI: 10.1039/d6py00313c

Poly(chromenochromenedione) (PCCD): a structural isomer of poly(benzodifurandione) (PBDF)

Uttam Pal, [a] Reed M. Woolard,[a] Priyanka Rout,[a] Sanket Samal, [a] Suman Kuila, [b] Md Masudur Rahman Rahat, [a] Guancheng Shen,[c] Julia Laskin, [a] Stephen Barlow, [b] Seth R. Marder, [b,d] Geoffrey R. Hutchison [c,e] and Jianguo Mei *[a]

Received 30th March 2026,
Accepted 14th May 2026

DOI: 10.1039/d6py00313c

rsc.li/polymers

Access to robust n-type conducting polymers remains a central challenge in advancing organic electronics. Recently, n-doped poly(benzodifurandione) (n-PBDF) has emerged as a solution-processable, air-stable, n-type conducting polymer, which exhibits exceptional properties in electronic, electrochemical, and mixed ionic-electronic devices. PBDF has a structural isomer, poly(chromenochromenedione) (PCCD), whose synthesis and properties have remained unexplored. Here, we report a synthetic strategy that enables the successful transformation of PBDF into its structural isomer, PCCD. The process proceeds *via* a two-step pathway: aqueous base induced ring opening of n-PBDF to yield a water soluble intermediate poly(phenylenediacetic acid) (PPDA), followed by acid mediated ring closure to form ladder type PCCD. The resulting polymer features fused coumarin units along its backbone, leading to an electronic structure and solid-state organization distinct from that of PBDF. A comparative study of these two isomeric polymers reveals pronounced differences in their structural, optoelectronic, and electrochemical characteristics.

Introduction

The development of solution processable, high conductivity n-doped conducting polymers has historically lagged behind that of their p-doped counterparts, primarily owing to challenges such as synthetic complexity and susceptibility to oxidative degradation by ambient oxygen and moisture.[1,2] However, recently n-doped poly(benzodifurandione) (n-PBDF) has emerged as a standout exception, demonstrating exceptional electrical conductivity and remarkable ambient stability.[3] These attributes are largely ascribed to its deep lowest unoccupied molecular orbital (LUMO) level (−4.90 eV as predicted by density functional theory (DFT) calculations), which thermodynamically stabilizes the n-doped state against oxidation. n-PBDF has already been integrated into various applications, including all-polymer transparent electrochromic displays and windows,[4,5] thermoelectric textiles,[6] solar cells,[7] organic batteries,[8] low-emissivity (low-e) paint[9] and OECTs.[10] While previous studies suggest that n-PBDF may isomerize into its structural isomer poly(chromenochromenedione) (PCCD) under certain conditions, an established experimental protocol to convert PBDF to PCCD has remained inaccessible (Fig. 1a).[11] Consequently, knowledge of PCCD has been confined to computational studies, which predicted notable differences relative to PBDF, including a shallower LUMO energy level (−4.51 eV *versus* −4.90 eV for PBDF) and a wider optical bandgap (1.95 eV *versus* 1.35 eV for PBDF).[12] Although the shallower LUMO energy level of PCCD may limit its n-doping efficiency and performance relative to PBDF, its significance lies in providing experimental access to the structural isomer of PBDF, enabling direct evaluation of backbone topology effects. The previous lack of experimental access to PCCD has hindered such a comparative study, leaving critical structure–property relationships unresolved and limiting the rational design of n-PBDF and related polymers with controlled doping behavior, stability, and processability.[13]

Here, we report the first isomerization of n-doped n-PBDF to PCCD *via* a two-step process. Aqueous base leads to ring

[a]*James Tarpo Jr. and Margaret Tarpo Department of Chemistry, Purdue University, West Lafayette, Indiana 47907, USA. E-mail: jgmei@purdue.edu*
[b]*Renewable and Sustainable Energy Institute, University of Colorado Boulder, Boulder, Colorado 80309, USA*
[c]*Department of Chemistry, University of Pittsburgh, Pittsburgh, Pennsylvania 15260, USA*
[d]*Department of Chemical and Biological Engineering, University of Colorado Boulder, Boulder, Colorado 80309, USA*
[e]*Department of Chemical and Petroleum Engineering, University of Pittsburgh, Pittsburgh, Pennsylvania 15261, USA*

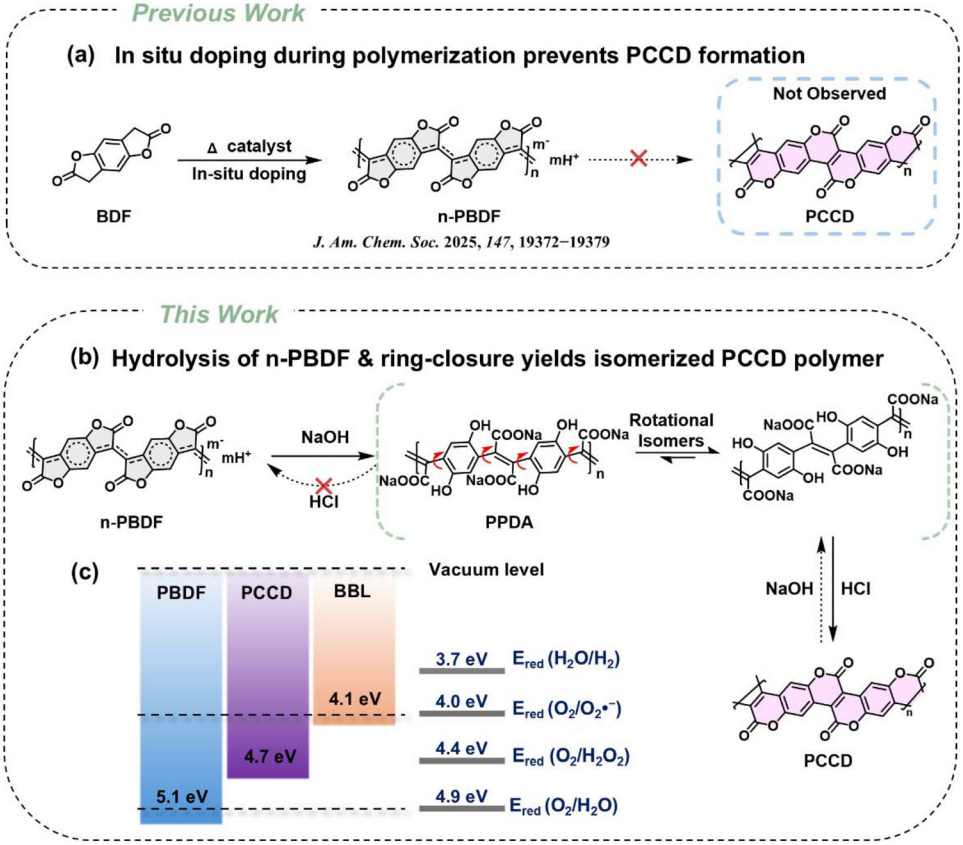

Fig. 1 (a) *In situ* doping prevents isomerization to PCCD during n-PBDF polymerization, (b) n-PBDF isomerization to its structural isomer PCCD *via* a two-step process, and (c) schematic representation of the LUMO energy level of PCCD compared to other conducting polymers.

opening hydrolysis, converting n-PBDF into poly(phenylenediacetic acid) (PPDA), disrupting the degree of conjugation and the doped state,[14] thereby enabling bond rotations toward a lower energy conformer (Fig. 1b). Subsequent acid mediated ring closure yields PCCD featuring six-membered coumarin rings, in contrast to the five-membered benzofuranone rings of PBDF. This synthetic methodology was first established using small, well-defined oligomer models before being extended to polymeric systems. The structural transformations were corroborated by nuclear magnetic resonance (NMR), ultraviolet–visible–near-infrared (UV–vis–NIR) spectroscopy, attenuated total reflectance–Fourier transform infrared (ATR–FTIR) spectroscopy, and Raman spectroscopy. In alignment with DFT calculations, PCCD shows a deeper LUMO level of −4.7 eV, comparable to other conducting polymers (Fig. 1c).[15] Although the rigid, ladder-like backbone of PCCD leads to poor intrinsic solubility,[16] we demonstrate two practical processing strategies. First, a solution processable n-doped PCCD (n-PCCD) ink in DMSO was obtained by blending with n-type dopants.[17,18] Second, the PCCD films were fabricated through *in situ* thin-film conversion of PPDA into PCCD and were further doped using a sequential doping strategy to obtain n-PCCD. Comparative evaluation of the two isomeric polymers (n-PBDF and n-PCCD) highlights how backbone topology dictates optoelectronic properties, solubility, and conductivity.

Results and discussion

Isomerization of discrete molecules and oligomers

To obtain molecular level insight into the structural isomerization of n-PBDF, we first investigated well-defined BDF based discrete molecules as model compounds before extending the isomerization strategy to the polymer system. A BDF based trimer (BFD_2) was synthesized and subjected to the same two-step isomerization protocol later applied to n-PBDF (Fig. 2a). Although elevated temperatures can induce isomerization in small molecule analogs, prior studies have shown that reductive doping of BDF based oligomers prevents isomerization, particularly for longer conjugated backbones.[19] All reactions were conducted in a DMSO/water mixed solution to emulate the hydrolysis environment of n-PBDF DMSO ink dispersion in water. Ring opening hydrolysis of BFD_2 was deliberately performed at room temperature to minimize potential side reactions, including unwanted doping or backbone degradation, which can occur in the presence of water at higher temperatures. UV–vis–NIR absorption spectroscopy was used to monitor the progress of the reaction. BFD_2 exhibits an absorption maximum at 563 nm which blue shifts to 297 nm after treatment with sodium hydroxide (NaOH), consistent with disruption of backbone planarity and loss of conjugation in the ring opened intermediate (PDA_2) (Fig. 2b). Following ring

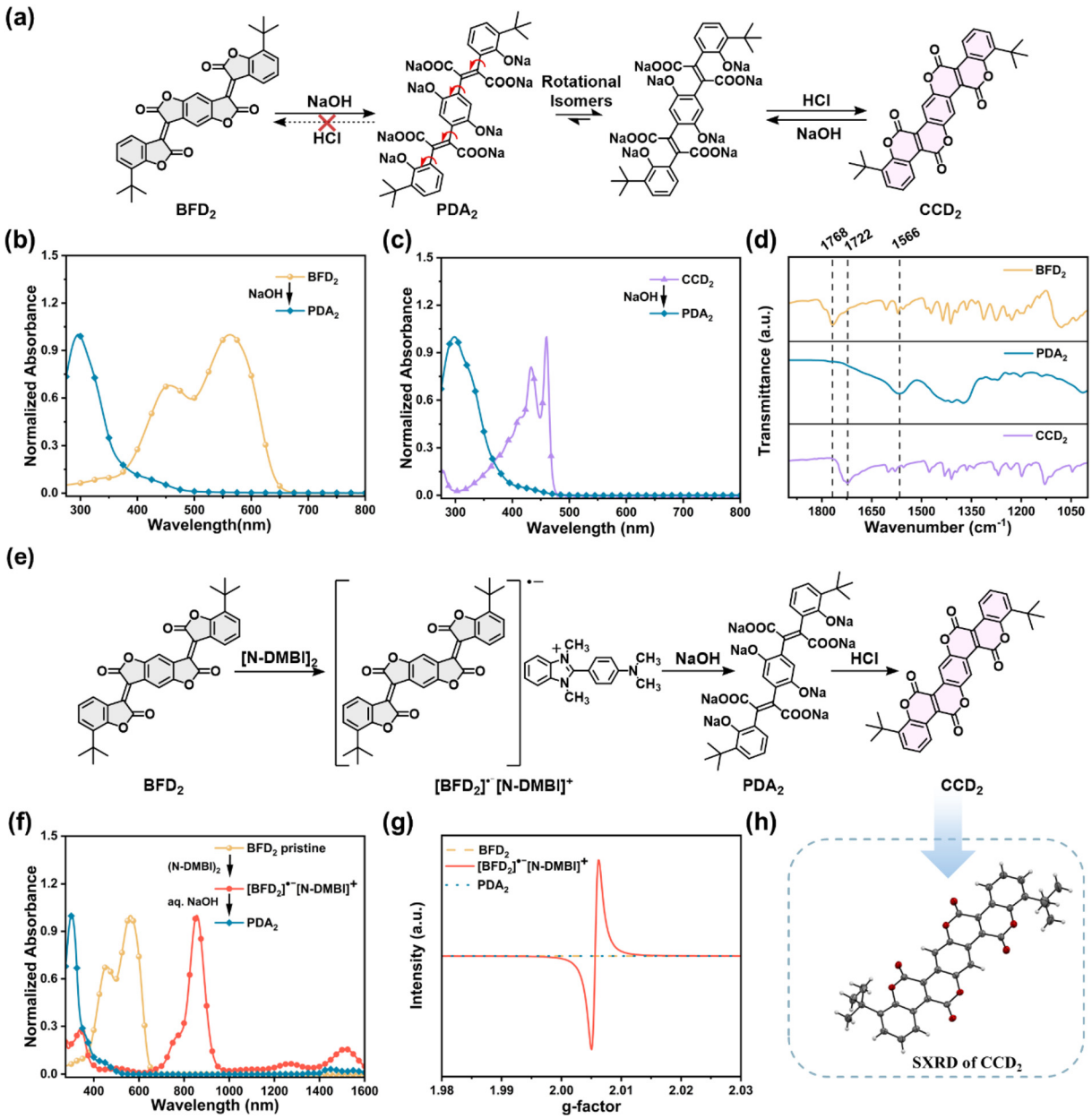

Fig. 2 (a) Isomerization of BFD_2 to CCD_2 in DMSO/water at room temperature *via* ring opening hydrolysis, (b) UV-vis-NIR absorption spectra of BFD_2 and hydrolyzed BFD_2 (PDA_2), (c) UV-vis-NIR absorption spectra of CCD_2 and hydrolyzed CCD_2 (PDA_2), (d) stacked FTIR spectra of BFD_2, PDA_2, and CCD_2, (e) n-doping of BFD_2 using $(N\text{-}DMBI)_2$ to obtain $[BFD_2]^{\bullet-}[N\text{-}DMBI]^+$, which was subjected to the two step isomerization process, (f) UV-vis-NIR absorption spectra of BFD_2, $[BFD_2]^{\bullet-}[N\text{-}DMBI]^+$, PDA_2 after hydrolysis of $[BFD_2]^{\bullet-}[N\text{-}DMBI]^+$, (g) EPR spectra of BFD_2, $[BFD_2]^{\bullet-}[N\text{-}DMBI]^+$, and PDA_2, and (h) SXRD structure of CCD_2.

opening hydrolysis of BFD_2, concentrated hydrochloric acid (HCl) was added to the reaction mixture, inducing six-membered lactone ring closure and precipitation of CCD_2. The structure of CCD_2 was confirmed by ^1H and ^{13}C NMR, ESI-MS, and single crystal X-ray (SXRD) analysis. To further probe the isomerization mechanism, the isolated CCD_2 was independently subjected to ring opening hydrolysis under identical conditions. The resulting product displayed absorption spectra identical to that obtained from BFD_2 hydrolysis, indicating the formation of the same ring opened species PDA_2 (Fig. 2c). To further confirm this mechanism, the base hydrolyzed product of small molecule dimers (BFD and CCD) were also characterized by *in situ* ^1H NMR and electrospray ionization mass spectrometry (ESI-MS) (Fig. S3 and S4), producing the same ring opened product. Subsequent acidification of the PDA_2 solution always regenerated CCD_2 instead of BFD_2. These results demonstrate that both BFD_2 and CCD_2 converge to a common ring opened species, which preferentially undergoes six-membered lactone ring closure upon acidification to yield the thermodynamically favored CCD_2 isomer.[20] The FTIR spectra

of BFD_2, the hydrolyzed species (PDA_2), and CCD_2 exhibit distinct features (Fig. 2d). BFD_2 and CCD_2 display characteristic C═O stretching bands at 1768 cm^{-1} and 1722 cm^{-1}, respectively, corresponding to five- and six-membered lactone rings. In contrast, these bands disappear in PDA_2, which instead shows a broad band at 1568 cm^{-1} assigned to asymmetric stretching of carboxylate (COO^-) groups, along with a broad O–H stretching band between 3700–3000 cm^{-1} arising from hydrogen bonding (Fig. S5). These spectral changes confirm complete ring opening of the lactone rings in both BFD_2 and CCD_2 to generate the same carboxylate containing species (PDA_2).

While ring opening hydrolysis was initially examined using neutral oligomeric models, n-PBDF exists in a highly doped state, with a reported doping level of ~0.9 electrons per repeating unit,[21] which prevents *in situ* structural isomerization during PBDF polymerization. To determine whether base mediated hydrolysis can also proceed on a doped backbone, we treated n-doped BFD_2 with aqueous NaOH (Fig. 2e). BFD_2 was chemically doped using the molecular n-type dopant $(N\text{-}DMBI)_2$ to generate the radical anion species $[BFD_2]^{\bullet-}$, with $N\text{-}DMBI^+$ serving as the countercation.[22] UV–vis–NIR spectroscopy in DMSO confirmed successful doping: neutral BFD_2 exhibits absorption bands at 456 and 563 nm, whereas doped $[BFD_2]^{\bullet-}$ displays a new red shifted band at 857 nm, with small peaks around 1267 and 1513 nm (Fig. 2f). Upon addition of aqueous NaOH to the solution of $[BFD_2]^{\bullet-}[N\text{-}DMBI]^+$, the characteristic doping related absorption peaks disappeared and were replaced by a blue shifted band at 302 nm, similar to that of the ring opened intermediate PDA_2 derived from neutral BFD_2. Subsequent acidification with HCl resulted in precipitation of the CCD_2 isomer. Electron paramagnetic resonance (EPR) spectroscopy further corroborated these assignments. The doped oligomer $[BFD_2]^{\bullet-}[N\text{-}DMBI]^+$ exhibits a strong EPR signal, whereas neutral BFD_2 and the hydrolyzed intermediate (PDA_2) are EPR silent, consistent with loss of unpaired spins upon hydrolysis (Fig. 2g). Furthermore, SXRD analysis on the isolated CCD_2 confirms the proposed isomerized six-membered lactone ring structure (Fig. 2h).

Isomerization of n-PBDF to PCCD

After establishing the feasibility of the two-step isomerization in oligomeric models, we extended this strategy to the n-PBDF polymer. The n-PBDF DMSO ink was hydrolyzed using 50 wt% NaOH (with respect to n-PBDF content) in a DMSO/water (1 : 7) dispersion at 100 °C for 7 h under nitrogen (Fig. 3a). UV–vis–NIR absorption spectroscopy revealed complete disappearance of the characteristic polaron and bi-polaron absorptions of n-PBDF in the NIR region, accompanied by the emergence of a new absorption band at 377 nm and a visible solution color change from black to yellow (Fig. 3a and b). Among the bases tested under the above conditions, only NaOH and Na_2CO_3 achieved complete hydrolysis of n-PBDF to PPDA (Fig. S6). After complete hydrolysis of n-PBDF, no further changes were observed in the UV-vis-NIR and FTIR spectra of PPDA upon prolonged exposure to NaOH, indicating that PPDA remains stable under strongly alkaline hydrolysis conditions (Fig. S7). Furthermore, EPR spectra showed considerably reduced polaron intensity, indicating almost complete loss of the n-doped state upon hydrolysis of n-PBDF (Fig. S8). Complementary FTIR and Raman analyses further confirm complete ring opening hydrolysis of the five-membered lactone rings along the PBDF backbone, generating a new polymer, poly(phenylenediacetic acid) (PPDA). Subsequently, concentrated HCl (20 vol% relative to the water content) was added, and the mixture was stirred at 100 °C for an additional 6 h.

During this acid mediated ring closing step, the PPDA polymer preferentially undergoes six-membered lactone formation to yield PCCD rather than reforming the five-membered PBDF isomer, similar to BDF based oligomeric molecules. PCCD, due to its limited solubility, precipitates out as a dark pink solid. The isolated polymer was further dispersed in DMSO to obtain a solution, and thin-film UV-vis-NIR absorption spectra (Fig. 3c and S9), showing similar absorption profiles. To further differentiate PCCD from PBDF, an n-PBDF thin film was chemically de-doped using Magic Blue.[23] The thin film absorption spectrum of PCCD displays a sharp peak at 560 nm with a shoulder at 517 nm, which is clearly distinct from that of neutral PBDF, which exhibits a broad absorption peak at 895 nm, indicating that our synthetic process results in structural isomerization rather than a de-doped n-PBDF. Among the acids tested under the same conditions, HCl and H_2SO_4 promoted efficient conversion of PPDA to PCCD. Importantly, all acid mediated ring-closure reactions consistently favored the formation of the six membered lactone ring, with no evidence for reformation of the five membered benzofuranone (Fig. S10). We also evaluated the effect of the DMSO/H_2O ratio on the two-step isomerization reaction of n-PBDF to PCCD. Among different solvent ratios, the DMSO/H_2O ratio of 1 : 7 led to the most efficient conversion to PCCD (Fig. S11).

PCCD structure characterization

The structural evolution of polymers during isomerization was examined using FTIR spectroscopy by comparing n-PBDF, PPDA, and PCCD (Fig. 3d). n-PBDF exhibits a characteristic lactone C═O stretching band at 1781 cm^{-1}. Upon hydrolysis, this band disappears in PPDA, accompanied by the emergence of new C═O stretching modes assigned to –COOH (1689 cm^{-1}) and $-COO^-$ (1584 cm^{-1}), along with a broad –OH stretching band spanning 3200–3600 cm^{-1} (Fig. S12).[24,25] These features indicated ring opening of the five-membered lactone rings throughout the PBDF backbone. In contrast, the FTIR spectrum of isolated PCCD displays a C═O stretching band at 1721 cm^{-1}, characteristic of six-membered lactone rings of the coumarin moiety.[26] For comparison, neutral PBDF exhibits a lactone C═O stretching band at 1769 cm^{-1}, further verifying that PCCD is chemically distinct from PBDF and not simply a de-doped product (Fig. S13). Raman spectroscopy further provides complementary evidence for backbone transformation during the two-step isomerization. In particular, the heterocyclic C–O–C stretching vibration serves as a sensitive

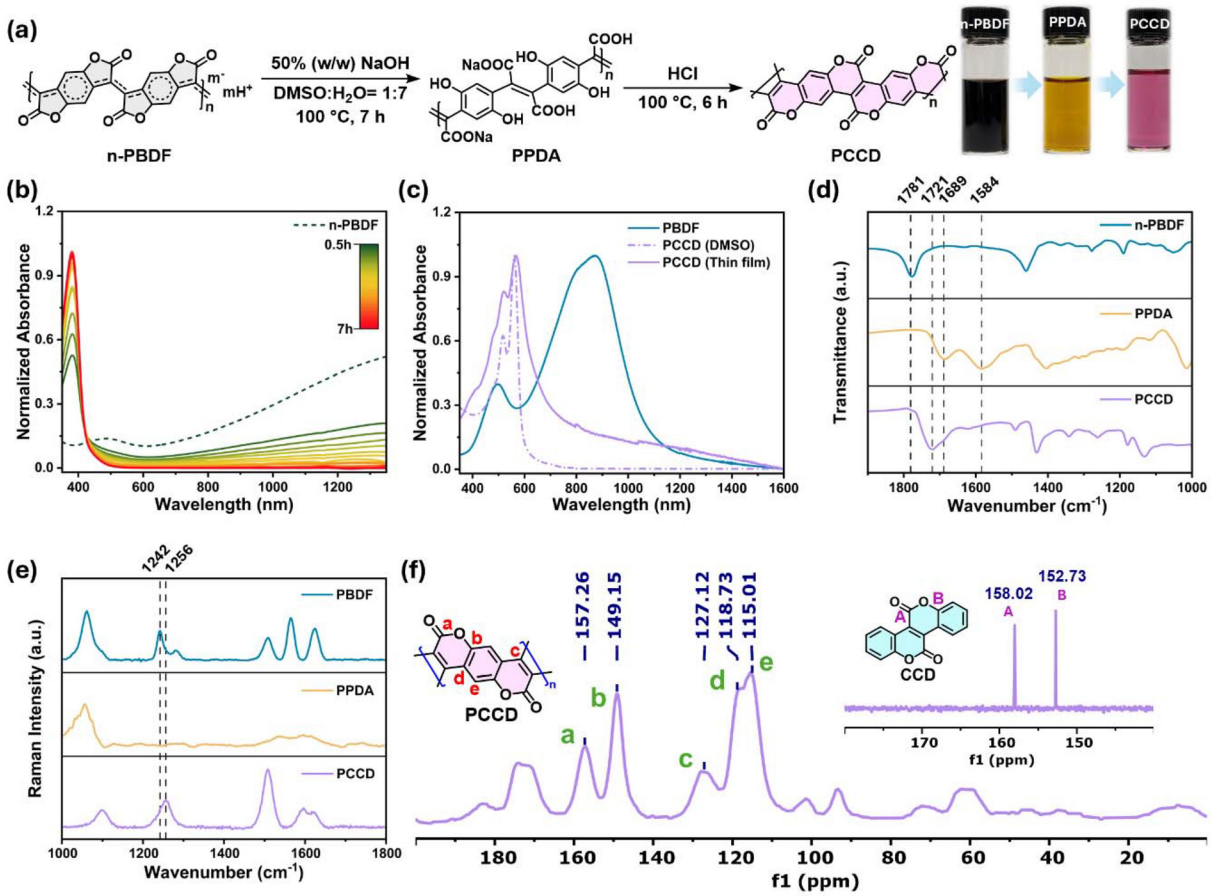

Fig. 3 (a) Isomerization of n-PBDF DMSO ink to PCCD, (b) time-dependent UV-vis-NIR absorption spectra of n-PBDF hydrolysis, (c) UV-vis-NIR absorption spectra of PBDF thin films compared with PCCD in solution and thin film states, (d) stacked FTIR spectra of n-PBDF, PPDA, and PCCD, (e) stacked Raman spectra of PBDF, PPDA, and PCCD, (f) solid-state ^{13}C CP-MAS NMR spectrum of PCCD (inset shows the zoomed in ^{13}C NMR spectrum of CCD showing the characteristic carbonyl assignment).

marker: the five-membered lactone C–O–C signal of PBDF at 1242 cm^{-1} disappears upon hydrolysis to PPDA and reappears at 1256 cm^{-1} upon ring closure to the six-membered lactone ring in PCCD (Fig. 3e), confirming the two-step ring opening and ring closing pathway.[27,28]

Solid-state ^{13}C NMR spectra of PCCD were obtained using cross-polarization magic-angle spinning (CP-MAS) techniques (Fig. 3f). The spectrum shows resonances exclusively above 90 ppm, consistent with the fully conjugated sp^2 carbon framework of the PCCD backbone.[29] The resonance at 157.26 ppm is assigned to the lactone carbonyl carbon of the coumarin moiety.[30] Signals at 149.15 ppm and 118.73 ppm are attributed to quaternary sp^2 aromatic carbons bonded to oxygen and carbon, respectively. The peak at 115.01 ppm corresponds to unsubstituted aromatic sp^2 carbons, while the resonance at 127.12 ppm is assigned to vinylic sp^2 carbons shared between adjacent coumarin units. DFT calculations of the ^{13}C NMR chemical shifts for the repeating unit of PCCD exhibit good agreement with the experimental spectrum (Fig. S14). Furthermore, the zoomed in ^{13}C NMR spectra of BFD and CCD establish the presence of six-membered lactone rings along the PCCD backbone, rather than five-membered lactone rings (Fig. S15). The ^{13}C NMR signal of carbonyl carbon in CCD was observed at 158.02 ppm, consistent with that of PCCD, whereas the corresponding carbonyl signal in BFD appears at 166.98 ppm. This suggests that PCCD exhibits no detectable structural defects within the sensitivity limits of these measurements, although minor defects below the detection limit cannot be excluded.[31] Additionally, the thermodynamically stable backbone of PCCD exhibits high thermal stability, with a 5% weight loss at >426 °C in thermogravimetric analysis (TGA) (Fig. S16).[32]

Solution processability of PCCD through n-doping

PCCD features a side-chain free, ladder-like backbone, resulting in poor solubility in common organic solvents, with limited solubility in DMSO (<0.1 mg mL^{-1}). This low solubility makes conventional solution processing impractical for device fabrication and other applications. To obtain a conductive, solution-processable ink, we employed a blend-doping strategy using the organic n-dopant (N-DMBI)$_2$ (Fig. 4a).[33] Upon heating a mixture of solid PCCD and (N-DMBI)$_2$ in DMSO at

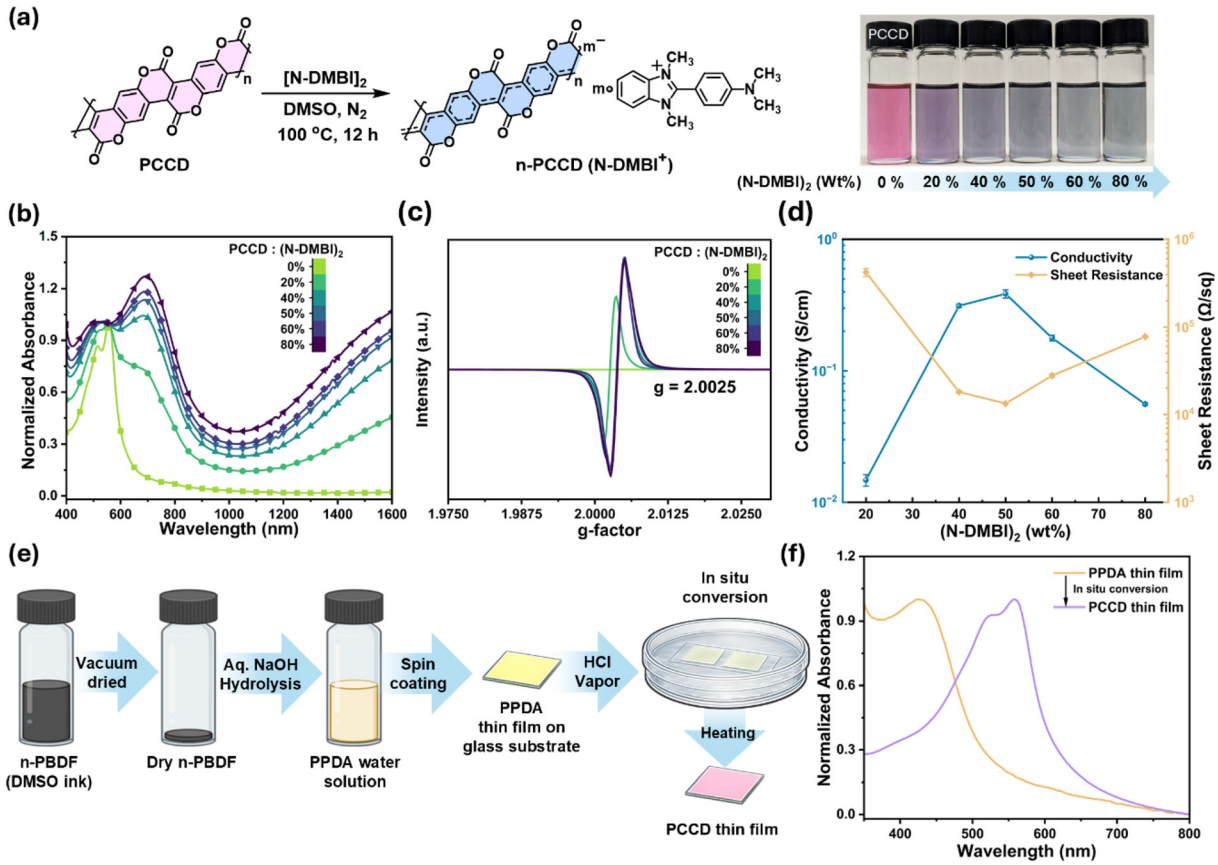

Fig. 4 (a) n-Doping of PCCD to n-PCCD with $(N\text{-}DMBI)_2$, (b) UV-vis-NIR absorption spectra of PCCD and n-PCCD under various dopant loading, (c) EPR spectra of PCCD and n-PCCD under various dopant loading at 20 K, (d) conductivity and sheet resistance of the n-PCCD films at different dopant loading, (e) schematic representation of water processed PCCD thin films, and (f) UV-vis absorption spectra of PPDA thin film and *in situ* converted PCCD thin film.

100 °C, efficient doping occurs, producing a dark-blue n-doped PCCD (n-PCCD) ink. UV–vis–NIR absorption spectra of n-PCCD solutions in DMSO reveal the emergence of a polaron absorption peak at ~710 nm along with pronounced absorption in the NIR region, consistent with successful doping (Fig. 4b and S17).[34] To further probe charge-carrier formation, EPR spectroscopy was performed on n-PCCD inks prepared with different dopant loadings. Strong EPR signals with a Landé *g*-factor of 2.0025 were observed, confirming the generation of polarons upon doping in n-PCCD (Fig. 4c). Moreover, chemical de-doping of n-PCCD thin films with $FeCl_3$ resulted in the disappearance of the n-PCCD NIR absorption band, accompanied by the reappearance of the neutral PCCD absorption band (Fig. S18). This spectral change suggests that the PCCD polymer backbone tolerates chemical doping and de-doping without obvious irreversible side reactions under these conditions.[35] In-plane electrical conductivity of drop casted n-PCCD films was measured using a four-point probe instrument, achieving a maximum conductivity of 0.38 ± 0.027 S cm^{-1} at 50 wt% $(N\text{-}DMBI)_2$ (Fig. 4d). The lower conductivity of n-PCCD compared to n-PBDF can be attributed to several factors: reduced charge carrier generation efficiency arising from the shallower LUMO level of PCCD (−4.51 eV) relative to PBDF (−4.90 eV) as predicted by DFT simulations, and disruption in polymer packing associated with the $N\text{-}DMBI^+$ counterions in n-PCCD *versus* H^+ in n-PBDF.[36,37]

Water processable PCCD thin film formation

Although PCCD is not directly solution-processable due to its side-chain free, ladder backbone, access to neutral thin films is highly desirable for various organic-electronic device applications. To overcome this limitation, we developed a water processable strategy that enables the formation of PCCD thin films *via in situ* ring closure of the water-soluble polymer PPDA (Fig. 4e). Solid n-PBDF powder was treated with aqueous NaOH at 100 °C for 2 h under nitrogen, resulting in complete hydrolysis of the five-membered lactone rings and formation of a yellow aqueous solution of PPDA, as confirmed by UV–vis–NIR and FTIR spectroscopy (Fig. S19). The PPDA solution was subsequently spin-coated onto glass substrates, and the resulting thin films were exposed to HCl vapor for a couple of minutes, followed by thermal annealing at 180 °C for 4 h to induce acid mediated ring closure, thereby generating PCCD directly in the solid state (thickness 40 nm to 50 nm). The

in situ conversion of PPDA to PCCD within the thin films was verified by UV–vis–NIR and FTIR analyses (Fig. 4f and S19), confirming successful formation of neutral PCCD films. The *in situ* converted PCCD thin films were further sequentially doped using $(N\text{-}DMBI)_2$ (solution in DMSO). The UV-vis-NIR absorption spectra revealed a pronounced decrease in the neutral PCCD absorption band with the concomitant rise of n-PCCD polaron absorption in the NIR region, consistent with that of blend doped n-PCCD (Fig. S20). The sequentially doped n-PCCD thin film exhibited a conductivity of 2.46 ± 0.37 S cm^{-1}, which is higher than that of the blend doped n-PCCD.

Thin-film morphology and electrochemistry

Atomic force microscopy (AFM) was employed to investigate the thin film surface morphology of n-PBDF and n-PCCD [50 wt% $(N\text{-}DMBI)_2$]. Both thin films exhibit fibrous morphology; n-PCCD thin films, however, show more aggregated surface morphology with visible pinhole defects compared to n-PBDF (Fig. 5a and b). This could also contribute to the observed reduced conductivity in n-PCCD thin films compared to n-PBDF. Additionally, the *in situ* formed neutral PCCD thin film exhibited a different surface morphology, with increased aggregation and root mean square (RMS) roughness compared to PPDA (Fig. S21). This strong aggregation of PCCD is attributed to its rigid, ladder-like structure, which promotes strong π–π interactions and interchain aggregation.[38] The electrochemical properties of PCCD were investigated by cyclic voltammetry (CV) of n-PCCD [50 wt% $(N\text{-}DMBI)_2$] thin films coated on ITO-coated glass substrate in a three-electrode setup using Ag/AgCl as the reference electrode (Fig. 5c and S22). The LUMO level of PCCD was estimated to be −4.7 eV, whereas that of PBDF is estimated to be −5.1 eV. Although the LUMO level of PCCD is shallower than that of PBDF, it remains sufficiently deep to support its potential as an n-type conjugated ladder polymer. Spectro-electrochemical studies also confirmed reversible electrochemical doping and de-doping behavior in the n-PCCD thin films (Fig. 5d).

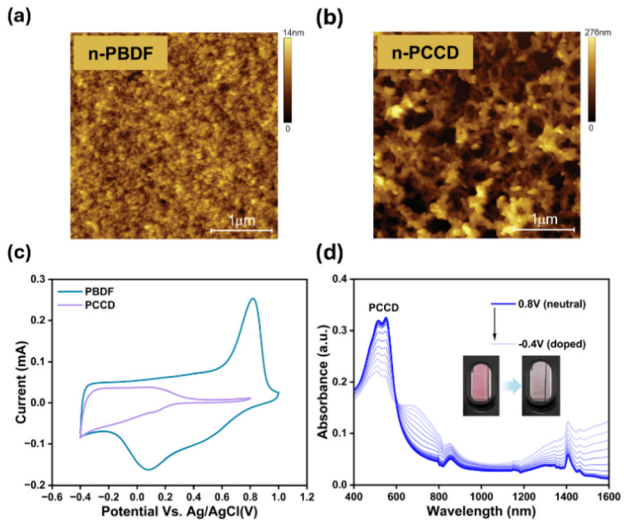

Fig. 5 AFM images of (a) n-PBDF thin film (RMS roughness = 1.72 nm), (b) n-PCCD (50 wt% $N\text{-}DMBI^+$) thin film (RMS roughness = 52.65 nm), (c) overlapping CV of PBDF and PCCD, and (d) spectro-electrochemistry of n-PCCD.

Conclusion

We report the first experimental formation of PCCD, a long-predicted structural isomer of PBDF, enabled by a two-step aqueous isomerization strategy. This approach proceeds through a common ring-opened PPDA polymer, followed by thermodynamically favored ring closure to form the ladder-type PCCD backbone. Direct comparison of PBDF and PCCD highlights the profound impact of backbone isomerism on conjugation, solubility, and conductivity. Beyond introducing PCCD as a new n-doped conducting polymer, this work demonstrates that post-synthetic structural isomerization can modulate PBDF polymer backbone structure and electronic properties without altering monomer composition.

Author contributions

J. M. conceived the project. U. P. designed and performed the experiments. R. M. W. assisted with the synthesis of monomers and small molecules. P. R. performed the electrochemical and spectro-electrochemical studies. S. S. assisted with AFM, data analysis, and contributed to manuscript preparation. S. K., S. B., and S. R. M. provided the n-type dopants. M. M. R. R. conducted mass spectrometry. J. L. supervised the mass analysis work. G. S. performed computational studies. G. R. H. supervised the computational work. U. P. wrote the original manuscript. U. P., S. S., and J. M. reviewed and edited the paper. J. M. supervised the project and provided overall guidance.

Conflicts of interest

Purdue University filed a patent disclosure (UP and JM). JM is a co-founder of Ambilight Inc. and founder of PBDF LLC. For the remaining authors, there are no conflicts to declare.

Data availability

The data supporting this article are included as part of the supplementary information (SI). Supplementary information: detailed experimental methods, synthetic procedures, characterization data (^{1}H NMR and ^{13}C NMR, UV-Vis, IR, EPR, and TGA spectra), AFM images, and computational details. See DOI: https://doi.org/10.1039/d6py00313c.

CCDC 2539281 for CCD_2 contains the supplementary crystallographic data for this paper.[39]

Acknowledgements

The authors would like to thank Dr John Harwood and Robert Santini NMR Facility at Purdue, for their assistance in acquiring the solid-state NMR data; Dr Hartmut Hedderich for their assistance in acquiring the TGA data; and Dr Matthias Zeller for their assistance in acquiring the crystallographic data. The authors would also like to thank Dr Bin Dong for their assistance in acquiring the Raman spectra. The authors would also like to thank Dr Jiao Suo for their assistance in acquiring polymer thin film thickness measurements. The authors would also like to thank Dr Michael Forrester Espenship and Bethany Ana Phillips for their assistance in analyzing the mass spectrometry data. This work was performed in part at the Research Instrument Center (RIC) of the Department of Chemistry, Purdue University. This project was supported by the Office of Naval Research (N00014-22-1–2177, Program Manager: Dr Paul Armistead).

References

1 X. Guo and A. Facchetti, *Nat. Mater.*, 2020, **19**, 922–928.
2 A. J. Heeger, *Angew. Chem., Int. Ed.*, 2001, **40**, 2591–2611.
3 H. Tang, Y. Liang, C. Liu, Z. Hu, Y. Deng, H. Guo, Z. Yu, A. Song, H. Zhao, D. Zhao, Y. Zhang, X. Guo, J. Pei, Y. Ma, Y. Cao and F. Huang, *Nature*, 2022, **611**, 271–277.
4 I. Song, W.-J. Lee, Z. Ke, L. You, K. Chen, S. Naskar, P. Mehra and J. Mei, *Nat. Electron.*, 2024, **7**, 1158–1169.
5 P. Rout, P. Mehra, W. Lee, L. You and J. Mei, *Adv. Funct. Mater.*, 2026, **36**, e31933.
6 M. Craighero, Q. Li, Z. Zeng, C. Choi, Y. Kim, H. Yoon, T. Liu, P. Sowinski, S. Haraguchi, B. Hwang, B. Mihiretie, S. Fabiano and C. Müller, *Adv. Sci.*, 2024, **11**, 2406770.
7 T. Liu, G. Beket, Q. Li, Q. Zhang, S. Y. Jeong, C. Yang, J. Huang, Y. Li, M. Stoeckel, M. Xiong, T. P. A. Van Der Pol, J. Bergqvist, H. Y. Woo, F. Gao, M. Fahlman, T. Österberg and S. Fabiano, *Adv. Sci.*, 2024, **11**, 2405676.
8 Z. Li, H. Tang, Y. Liang, Y. Liu, M. Li, L. Ma, H. Chen, X. Zhai, X. Wei, M. D. Gu, J. Wang, Y. Wang, S. Tong, Q. Jiang, Y. Geng, Y. Ma, Y. Cao, Y. Xu and F. Huang, *Nature*, 2026, **651**, 100–106.
9 X. Liu, W. Lee, D. W. Carne, Y. Tian, A. Felicelli, Y. Lei, J. A. Romo, L. You, Z. Xiong, O. G. R. Gonzalez, A. Aljwirah, Q. Gan, J. Mei and X. Ruan, *Adv. Funct. Mater.*, 2025, **36**, 2419685.
10 I. Sanjuán, D. Franco, Q.-G. Chen, C.-C. Chueh, W.-Y. Lee and A. Guerrero, *ACS Energy Lett.*, 2025, 5209–5217.
11 H. Ji, J. G. Lee, H. Lee, D. Kim and K. Cho, *Mater. Horiz.*, 2025, **12**, 9250–9261.
12 Z. Ke, A. Abtahi, J. Hwang, K. Chen, J. Chaudhary, I. Song, K. Perera, L. You, K. N. Baustert, K. R. Graham and J. Mei, *J. Am. Chem. Soc.*, 2023, **145**, 3706–3715.
13 M. T. Unruh, G. Wen, M. Bonn, S. Osella, H. I. Wang and U. Scherf, *Macromolecules*, 2024, **57**, 6390–6395.
14 Q. Li, J.-D. Huang, T. Liu, T. P. A. Van Der Pol, Q. Zhang, S. Y. Jeong, M.-A. Stoeckel, H.-Y. Wu, S. Zhang, X. Liu, H. Y. Woo, M. Fahlman, C.-Y. Yang and S. Fabiano, *J. Am. Chem. Soc.*, 2024, **146**, 15860–15868.
15 S. Griggs, A. Marks, H. Bristow and I. McCulloch, *J. Mater. Chem. C*, 2021, **9**, 8099–8128.
16 J. S.-J. Yang and L. Fang, *Chem*, 2024, **10**, 1668–1724.
17 H. Un, S. A. Gregory, S. K. Mohapatra, M. Xiong, E. Longhi, Y. Lu, S. Rigin, S. Jhulki, C. Yang, T. V. Timofeeva, J. Wang, S. K. Yee, S. Barlow, S. R. Marder and J. Pei, *Adv. Energy Mater.*, 2019, **9**, 1900817.
18 C.-Y. Yang, M.-A. Stoeckel, T.-P. Ruoko, H.-Y. Wu, X. Liu, N. B. Kolhe, Z. Wu, Y. Puttisong, C. Musumeci, M. Massetti, H. Sun, K. Xu, D. Tu, W. M. Chen, H. Y. Woo, M. Fahlman, S. A. Jenekhe, M. Berggren and S. Fabiano, *Nat. Commun.*, 2021, **12**, 2354.
19 J. Hwang, Q. Zhao, M. Ahmed, A. C. Yakisan, M. F. Espenship, J. Laskin, B. M. Savoie and J. Mei, *Angew. Chem., Int. Ed.*, 2024, **63**, e202401465.
20 H. D. Becker and H. Lingnert, *J. Org. Chem.*, 1982, **47**, 1095–1101.
21 S. Kang, E. C. Kim, H. W. Kim and B. Kang, *Macromol. Res.*, 2025, **33**, 377–383.
22 M. H. Ahmed, J. Hwang, B. Xiao, M. R. Schiavone, J. Chaudhary, M. Chen and J. Mei, *Macromolecules*, 2024, **57**, 10717–10724.
23 Z. Ke, J. Chaudhary, L. Q. Flagg, K. N. Baustert, A. O. Yusuf, G. Liu, L. You, K. R. Graham, D. M. DeLongchamp and J. Mei, *Adv. Funct. Mater.*, 2024, **34**, 2400255.
24 A. A. Korotkevich, C. J. Moll, J. Versluis and H. J. Bakker, *J. Phys. Chem. B*, 2023, **127**, 4544–4553.
25 J.-J. Max and C. Chapados, *J. Phys. Chem. A*, 2004, **108**, 3324–3337.
26 H. Zhang, Z. Zhou, C. Zhu and O. M. Yaghi, *Nat. Synth.*, 2025, **4**, 1376–1385.
27 D. Ohayon, G. Quek, B. R. P. Yip, F. Lopez-Garcia, P. R. Ng, R. J. Vázquez, D. V. Andreeva, X. Wang and G. C. Bazan, *Adv. Mater.*, 2024, **36**, 2410512.
28 J. Binoy, J. P. Abraham, I. H. Joe, V. George, V. S. Jayakumar, J. Aubard and O. F. Nielsen, *J. Raman Spectrosc.*, 2005, **36**, 63–72.
29 M. Odziomek, P. Giusto, J. Kossmann, N. V. Tarakina, J. Heske, S. M. Rivadeneira, W. Keil, C. Schmidt, S. Mazzanti, O. Savateev, L. Perdigón-Toro, D. Neher, T. D. Kühne, M. Antonietti and N. López-Salas, *Adv. Mater.*, 2022, **34**, 2206405.
30 H. Duddeck and M. Kaiser, *Org. Magn. Reson.*, 1982, **20**, 55–72.
31 J. Lee, A. J. Kalin, T. Yuan, M. Al-Hashimi and L. Fang, *Chem. Sci.*, 2017, **8**, 2503–2521.
32 W. Kong, X. Lu, H. Tang, K. Tan, Y. Wang, M. Zhang, S. Zhao, X. Zhang, F. Huang and Y. Feng, *Chem. Eng. J.*, 2026, **530**, 173464.
33 S. Jhulki, H.-I. Un, Y.-F. Ding, C. Risko, S. K. Mohapatra, J. Pei, S. Barlow and S. R. Marder, *Chem*, 2021, **7**, 1050–1065.

34 I. Zozoulenko, A. Singh, S. K. Singh, V. Gueskine, X. Crispin and M. Berggren, *ACS Appl. Polym. Mater.*, 2019, **1**, 83–94.
35 J. Hwang, X. Ni, M. F. Espenship, K. Tang, J. Zhang, A. Basu, S. Kuila, S. Barlow, S. R. Marder, J.-L. Brédas, J. Laskin and J. Mei, *J. Am. Chem. Soc.*, 2025, **147**, 19372–19379.
36 M. Xiong, X.-Y. Deng, S.-Y. Tian, K.-K. Liu, Y.-H. Fang, J.-R. Wang, Y. Wang, G. Liu, J. Chen, D. R. Villalva, D. Baran, X. Gu and T. Lei, *Nat. Commun.*, 2024, **15**, 4972.
37 C.-Y. Yang, Y.-F. Ding, D. Huang, J. Wang, Z.-F. Yao, C.-X. Huang, Y. Lu, H.-I. Un, F.-D. Zhuang, J.-H. Dou, C. Di, D. Zhu, J.-Y. Wang, T. Lei and J. Pei, *Nat. Commun.*, 2020, **11**, 3292.
38 G. Ma, M. Leng, S. Li, Z. Cao, Y. Cao, D. P. Tabor, L. Fang and X. Gu, *J. Mater. Chem. C*, 2022, **10**, 13896–13904.
39 M. Zeller, U. Pal and J. Mei, CCDC 2539281: Experimental Crystal Structure Determination, 2026, DOI: 10.5517/ccdc.csd.cc2r7b9n.